SUPERCONDUCTIVITY

Incoherent strange metal sharply bounded by a critical doping in Bi22 2

Su-Di Chen[1][2]* Makoto Hashimoto[3]* Yu He[1][2] Dongjoon Song[4]‡ Ke-Jun Xu[1] Jun-Feng He[1][2]§ Thomas P. Devereaux[2][5] Hiroshi Eisaki[4] Dong-Hui Lu[3] Jan Zaanen[1][6] Zhi-Xun Shen[1][2]

In normal metals, macroscopic properties are understood using the concept of quasiparticles. In the cuprate high-temperature superconductors, the metallic state above the highest transition temperature is anomalous and is known as the strange metal." We studied this state using angle-resolved photoemission spectroscopy. With increasing doping across a temperature-independent critical value $_c$ ~ 0.19, we observed that near the Brillouin zone boundary, the strange metal, characterized by an incoherent spectral function, abruptly reconstructs into a more conventional metal with quasiparticles. Above the temperature of superconducting fluctuations, we found that the pseudogap also discontinuously collapses at the very same value of $_c$. These observations suggest that the incoherent strange metal is a distinct state and a prerequisite for the pseudogap; such findings are incompatible with existing pseudogap quantum critical point scenarios.

andau s theory of Fermi liquids successfully explains the behavior of interacting electrons in normal metals. In a Fermi liquid, electronic states evolve adiabatically with increasing electron-electron interactions. Therefore, they remain in a one-to-one correspondence with the states in a Fermi gas and can be described in the language of quasiparticles. Soon after the discovery of cuprate high–transition temperature high-T_c) superconductors, it was realized that the cuprates fall into a different regime 1). The starting point is a Mott insulator with one hole per Cu site. The holes are localized thanks to strong on-site Coulomb repulsion and become mobile with increasing doping. At the optimal doping where T_c is maximized, the metallic state above T_c breaks the Fermi liquid rules 1–3). With sufficient overdoping, a key aspect of Fermi liquid behavior is eventually recovered: Quasiparticles have been directly observed by angle-resolved photoemission spectroscopy ARPES), spanning up a genuine Fermi

[1]Departments of Applied Physics and Physics, Stanford University, Stanford, CA 94305, USA. [2]Stanford Institute for Materials and Energy Sciences, SLAC National Accelerator Laboratory and Stanford University, Menlo Park, CA 94025, USA. [3]Stanford Synchrotron Radiation Lightsource, SLAC National Accelerator Laboratory, Menlo Park, CA 94025, USA. [4]National Institute of Advanced Industrial Science and Technology, Tsukuba, Ibaraki 305-8568, Japan. [5]Department of Materials Science and Engineering, Stanford University, Stanford, CA 94305, USA. [6]Institute Lorentz for Theoretical Physics, Leiden University, 2300 RA Leiden, Netherlands.
*These authors contributed equally to this work. †Present address: Department of Physics, University of California, Berkeley, CA 94709, USA. ‡Present address: Center for Correlated Electron Systems, Institute for Basic Science, Seoul 08826, Republic of Korea. §Present address: Department of Physics, University of Science and Technology of China, Hefei 230026, China.
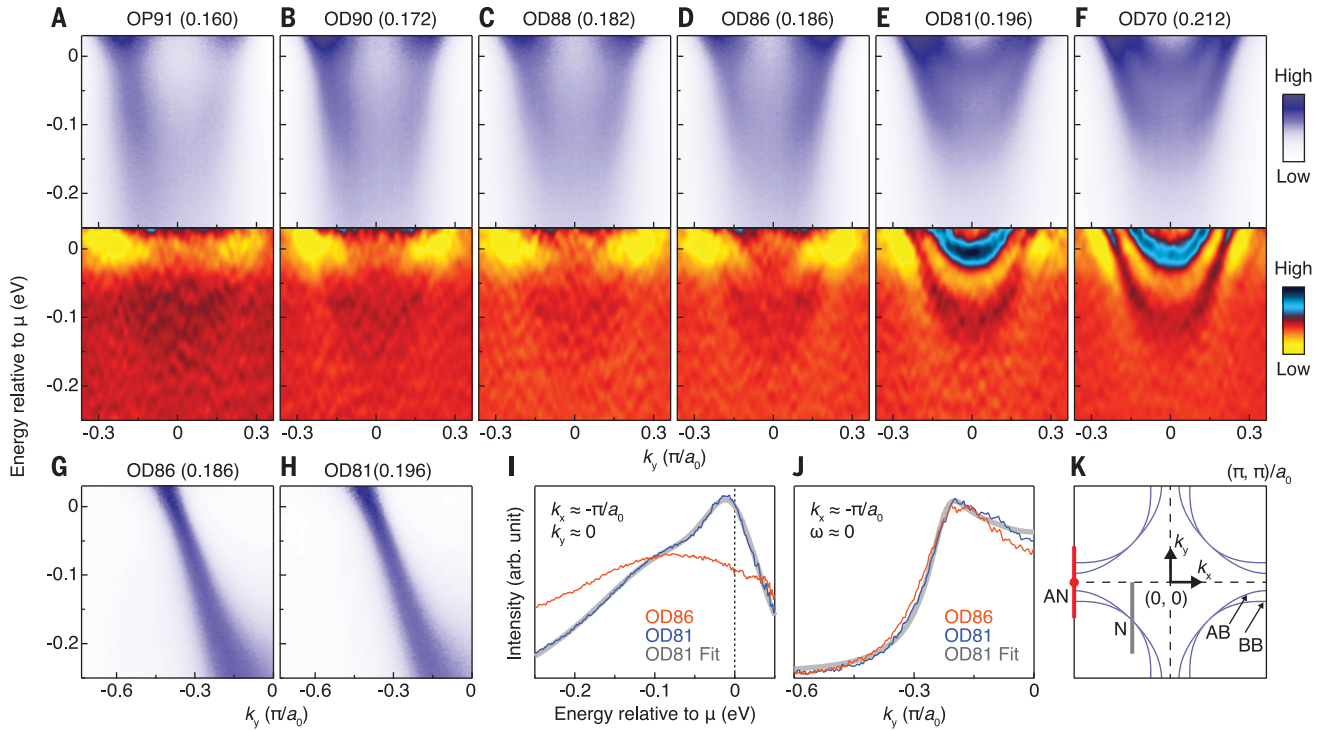Corresponding author. Email: zxshen@stanford.edu

surface 4–6). Here, we report the surprising way in which these quasiparticles spring into existence in Bi,Pb)$_2$Sr$_2$CaCu$_2$O$_{8+\delta}$ Bi2212), one of the most studied high-T_c superconductors.

We performed ARPES measurements over a wide temperature range on Bi2212 single crystals in fine doping steps. Such measurements are challenging because the increased outgassing from the sample environment at high temperature can easily contaminate the sample surface and alter the signal, given the small probe depth of ultraviolet photoemission. To overcome this problem, we controlled the sample temperature using a local heater and preserved the sample environment as a cold trap for contaminants throughout the measurements 7, 8). The spectra showed good consistency before and after thermal cycles between cryogenic and room temperatures fig. S1), which has rarely been demonstrated in prior work.

In Fig. 1, A to F, we show the doping evolution of the ARPES spectra collected at 250 K along the Brillouin zone BZ) boundary. On the heavily overdoped side, the spectra feature two parabolic-like dispersions known as the antibonding band AB) and bonding band BB) 3), consistent with band structure predictions for CuO$_2$ bilayers. However, once the doping level drops below p_c ~ 0.19, the spectra markedly broaden and dispersions are no longer identifiable. In Fig. 1, G and H, we also present the nodal spectra immediately below and above p_c, respectively. These two spectra show similar dispersions with almost identical sharpness, indicating that the change across p_c is intrinsic to the antinode and highly anisotropic.

We now try to understand this change in quasiparticle terms. In Fermi liquid–like sys-

tems, quasiparticles appear as poles in the spectral function,

$$A(k \omega = \frac{1}{\pi} \text{Im} \left[\frac{1}{\varepsilon_k - \omega + \Sigma(k \omega)} \right] \quad (1$$

where ω is the energy, k is the momentum, ε_k is the bare band dispersion, and $\Sigma k, \omega)$ is the perturbative self energy that captures interaction effects. For Bi2212, it has been reported that the normal-state self energy takes the marginal Fermi liquid form 9, 1):

$$\Sigma(k \omega = \lambda \left[\omega \ln\left(\frac{x}{\omega_c}\right) - i\left(\frac{\pi}{2}\right)x \right] - i\Gamma_0 \quad (2$$

with

$$x = \overline{\omega^2 + \pi^2 k_B^2 T^2} \quad (3$$

where λ is a coupling constant, ω_c is a cutoff energy, Γ_0 is an energy-independent scattering rate, k_B is the Boltzmann constant, and T is the absolute temperature. Immediately above p_c, we indeed find that the energy distribution curve EDC) at $-\pi, 0)/a_0$ antinode; a_0 is the unit cell dimension) can be well fitted using this self energy Fig. 1I) 8). Furthermore, the same set of parameters also reasonably describes the momentum distribution curve MDC) Fig. 1J) 8). In contrast, below p_c, the fitting becomes unstable as the antinodal EDC abruptly broadens and the quasiparticle peaks are replaced by an incoherent continuum Fig. 1I). Intriguingly, no substantial change is observed in the MDC linewidth across p_c Fig. 1J and fig. S2). This indicates that the disappearance of quasiparticle peaks is not a consequence of trivial elastic impurity scattering.

To further reveal the distinct spectral properties below and above p_c, we show the temperature dependence of spectra in Fig. 2 see fig. S3 for the complete dataset). Upon cooling, the antinodal EDC below p_c gains two important features with well-separated temperature scales Fig. 2A). The first is the pseudogap 2, 3), a low-energy spectral intensity depletion that gradually develops from far above T_c red arrow; see also Fig. 3A). The second is the Bogoliubov quasiparticle BQP) peak, which emerges as an intensity shoulder around 130 K and rapidly grows into a sharp peak with further decreasing temperature blue stripe). These two features are further accentuated by the temperature difference spectra, where the pseudogap manifests as a spectral weight transfer from near the chemical potential to a wide energy window Fig. 2B), and the BQP arises as a rather flat dispersion in a temperature range moderately above T_c Fig. 2C).

In contrast to the two-temperature-scale behavior below p_c, we find a more conventional

Fig. 1. Doping dependence of the electronic structure at 250 K in Bi2212.
(**A** to **F**) ARPES spectra (top) and their second energy derivatives (bottom) at six doping levels, taken along the Brillouin zone (BZ) boundary as indicated by the red line in (K); a_0 is the unit cell dimension. The corresponding sample (doping p) is marked at the top of each panel. Samples are named by their transition temperatures (T_c, in kelvin) rounded to the nearest integer with the prefix OD for overdoped and OP for optimally doped. The critical doping p_c is between OD86 and OD81. All data are divided by the resolution-convolved Fermi function. (**G** and **H**) ARPES spectra near the node (N) along the gray line in (K) from OD86 and OD81, respectively. (**I** and **J**) Energy distribution curves (EDCs) at the antinode [AN, red dot in (K)], and momentum distribution curves (MDCs) along the BZ boundary at the chemical potential μ, respectively. A momentum-independent background is subtracted (8). Curves are normalized by the area under them in the plotted horizontal axis range for better comparison. Data from OD81 are fitted to a marginal Fermi liquid model (8–10), and the results are plotted in gray. (**K**) Schematics of the Fermi surfaces formed by the antibonding band (AB) and bonding band (BB) in the first BZ.
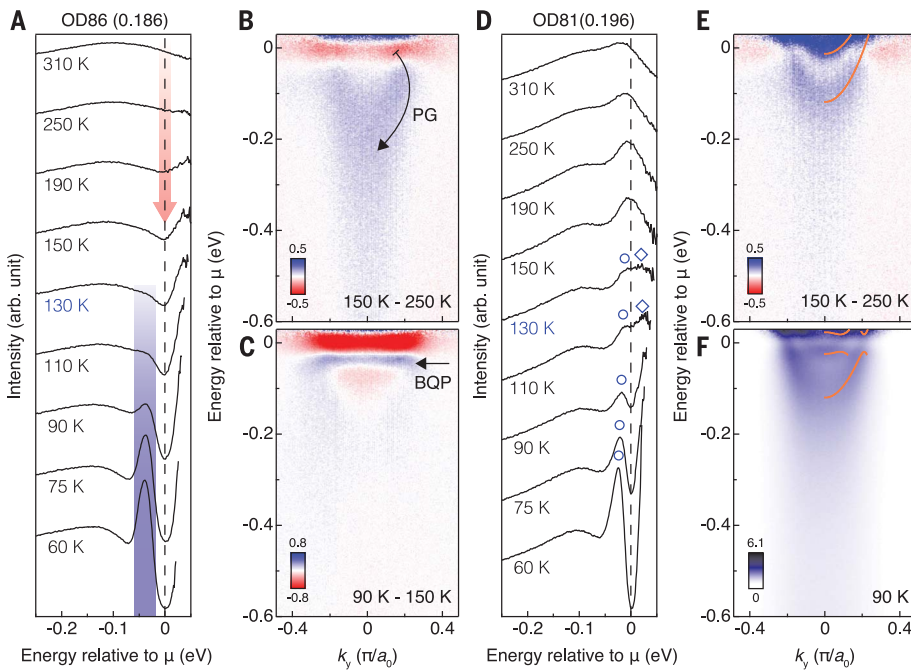

Fig. 2. Temperature dependence of the electronic structure immediately below and above T_c.
(**A**) Temperature evolution of antinodal EDCs in OD86 ($p \sim 0.186$). The curves are offset for clarity. The red arrow indicates the development of the pseudogap (PG). The blue stripe highlights the intensity shoulder and its evolution into the sharp Bogoliubov quasiparticle (BQP) peak. All data are divided by the Fermi function. (**B**) Difference between the ARPES spectra taken at 150 K and 250 K along the BZ boundary in OD86. The original spectra at each temperature are normalized such that the average intensity between −0.6 and −0.5 eV equals 1. The black arrow indicates the spectral weight transfer due to the PG. (**C**) Same as (B) but between spectra taken at 90 K and 150 K. The black arrow highlights the emergence of the BQP. (**D** and **E**) Same as (A) and (B) but taken for OD81 ($p \sim 0.196$). The open diamonds and circles in (D) are guides to the eye and denote the BQP peaks above and below the chemical potential, respectively. (**F**) ARPES spectra taken at 90 K along the BZ boundary in OD81. The orange curves in (E) and (F) are guides to the eye and highlight the normal quasiparticle and BQP dispersions, respectively.

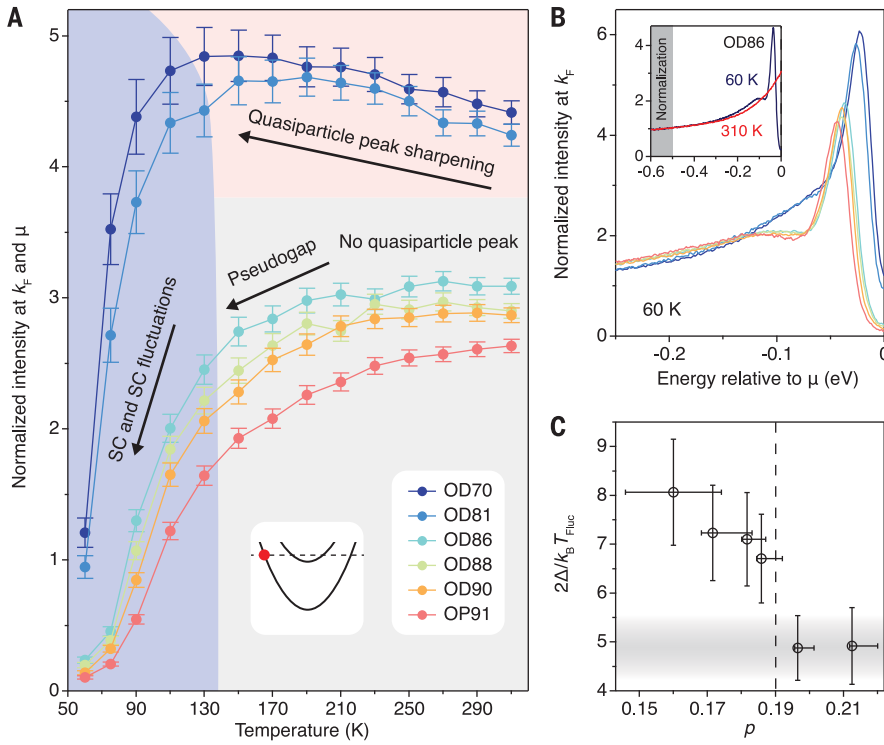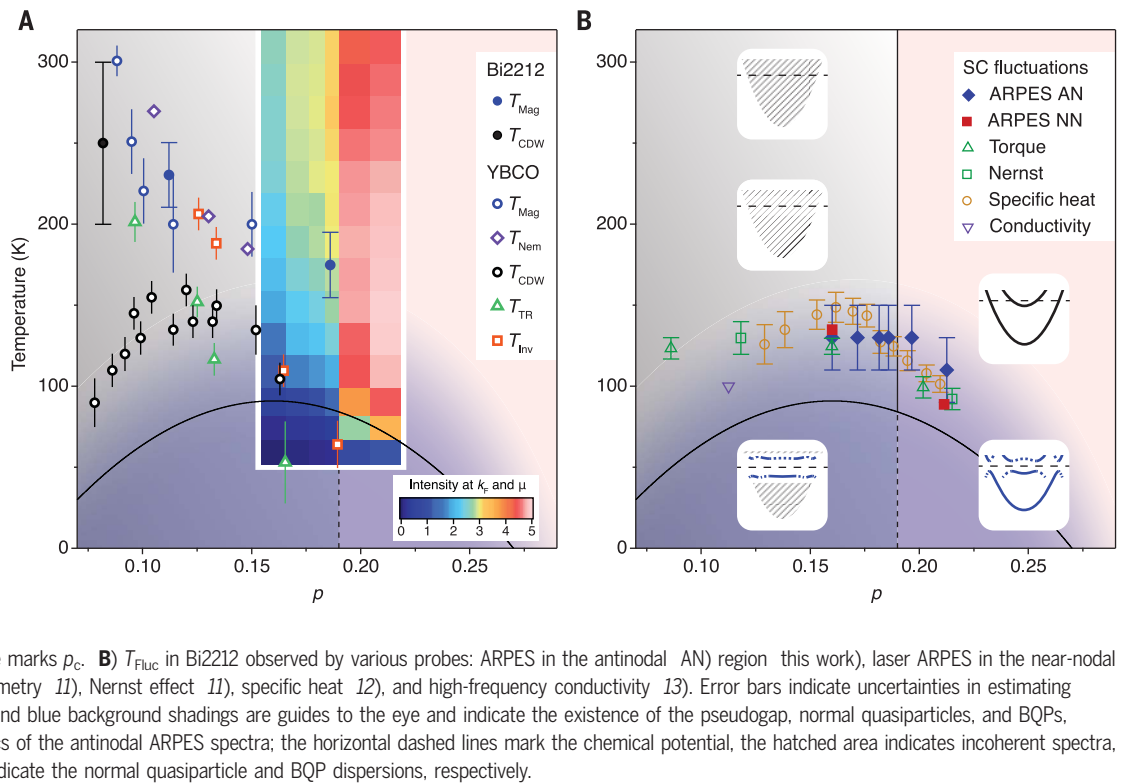**Fig. 3. Marked changes of spectral properties across T_c.** **A**) Temperature dependence of spectral intensity at the BZ-boundary BB Fermi momentum (k_F and μ; red dot in inset). The error bars reflect the noise level in the ARPES data and uncertainties in determining k_F and μ. **B**) Doping evolution of EDCs at the BZ-boundary BB k_F and 60 K. All data in A) and B) are background-subtracted (8), divided by the Fermi function, and normalized such that the average EDC intensity between −0.6 and −0.5 eV equals 1. The inset shows examples of intensity normalization using OD86 data. **C**) Doping dependence of $2\Delta/k_B T_{Fluc}$, where Δ is the antinodal superconducting gap size, k_B is the Boltzmann constant, and T_{Fluc} is the temperature scale of superconducting fluctuations. The horizontal error bars are caused by uncertainties in T_c measurements; the vertical error bars reflect uncertainties in determining Δ and T_{Fluc}.

Fig. 4. Phase diagram of Bi2212. **A**) The color plot (outlined in white) shows the spectral intensity at the BZ-boundary BB k_F and μ (same data as in Fig. 3A) plotted as a function of both temperature and doping. For $p < p_c$, this intensity reduces with decreasing temperature and doping, reflecting the development of the pseudogap. Also plotted are the transition temperatures of various broken symmetries in Bi2212 and YBa$_2$Cu$_3$O$_{6+\delta}$ (YBCO): magnetic order (T_{Mag}, 24–26), charge order (T_{CDW}, 27–29), nematicity (T_{Nem}, 30), time-reversal symmetry breaking (T_{TR}, 31), and inversion-symmetry breaking (T_{Inv}, 32). The black curve marks T_c; the vertical dashed line marks p_c. **B**) T_{Fluc} in Bi2212 observed by various probes: ARPES in the antinodal (AN) region (this work), laser ARPES in the near-nodal (NN) region (7), torque magnetometry (11), Nernst effect (11), specific heat (12), and high-frequency conductivity (13). Error bars indicate uncertainties in estimating these temperatures. Gray, pink, and blue background shadings are guides to the eye and indicate the existence of the pseudogap, normal quasiparticles, and BQPs, respectively. Insets are schematics of the antinodal ARPES spectra; the horizontal dashed lines mark the chemical potential, the hatched area indicates incoherent spectra, and the black and blue curves indicate the normal quasiparticle and BQP dispersions, respectively.

temperature evolution above p_c. With decreasing temperature, the quasiparticle peaks first sharpen with no sign of the pseudogap (Fig. 2, D and E, and Fig. 3A). Then at around 130 K, a gap opens with the rise of one additional peak.

The peak can be attributed to the back-bending AB above the chemical potential (Fig. 2, D and F), consistent with the formation of BQP dispersions when a superconducting gap opens. With further decreasing temperature, the gap and low-energy peaks become more prominent. Yet as superconductivity develops, no other major changes are observed in the electronic structure. These observations imply that both the gaps above and below T_c here

are associated with superconductivity. The absence of additional gap-like features also indicates that the pseudogap suddenly collapses at p_c with overdoping. Furthermore, by following the BQP shoulder for doping $p < p_c$ and the gap above T_c for $p > p_c$ figs. S3 and S4), we establish a temperature scale for superconducting fluctuations, T_{Fluc}, that smoothly follows the T_c dome. This is consistent with results from other studies [7, 11–13], as summarized in Fig. 4B.

We further compare the spectra across p_c in the superconducting state. In Fig. 3B we show the doping dependence of EDCs at 60 K, a temperature where the growth of the superconducting gap is almost complete [14]. These EDCs are taken from the BB Fermi momentum to minimize bilayer effects. Below p_c, the EDCs exhibit the anomalous peak-dip-hump line shape, and the gap-to-T_{Fluc} ratio gradually decreases with increasing doping Fig. 3C). Once above p_c, we find that the dip rapidly weakens and the gap-to-T_{Fluc} ratio saturates. These changes reflect the impact of the normal state on the superconducting phase, echoing previous observations of low-temperature anomalies across the very same p_c [14-2).

We now discuss the implications of our results. Previously, the low-temperature anomalies at p_c were sometimes viewed as evidence of a conventional order undergoing a continuous quantum phase transition. In this picture, the order parameter would couple to the electrons and cause the pseudogap, and its quantum critical fluctuations would give rise to the strange metal within a V-shaped region in the temperature-doping phase diagram [1]. However, this scenario is hard to reconcile with several studies in the normal state, where the experimental observations are indicative of a change of quasiparticle coherence across p_c at elevated temperatures [15, 21–23]. Consistent with these studies, our data provide direct microscopic evidence that p_c is not associated with a V-shaped quantum critical region, but instead represents a temperature-independent boundary between the incoherent strange metal and the overdoped quasiparticle metal. Furthermore, we find that upon cooling, the pseudogap develops only inside the incoherent strange metal and in turn serves as a parent state for various broken symmetries that occur at even lower temperatures Fig. 4A) [24–32]. These observations suggest that the pseudogap is a subordinate phenomenon to the incoherent strange metal and does not form a quantum critical point.

A remaining puzzle is the incoherent antinodal line shape. It has been suggested that incoherence may arise from strong coupling between electrons and bosonic modes such as spin excitations [4] and phonons

[33, 34]. However, this alone cannot produce the discontinuous change of spectral function at p_c. In fact, as the impact of this change persists to high energy and temperature, conventionally it would be associated with a first-order phase transition. One possibility is the involvement of a structural transition. For example, an abrupt change of CuO_2 plane dimpling has been reported in $YBa_2Cu_3O_{6+\delta}$ near optimal doping [35]. Yet it remains to be seen whether a similar structural transition happens at p_c in Bi2212 and strongly affects the bare band dispersions and mode coupling properties. Moreover, certain short-range orders, such as the short-range charge density wave [14] and nematic glass [36], may also contribute to the broadening of antinodal spectra. Considering these factors, it seems possible that our data can be explained by a conventional theory. However, such explanations become debatable when results from other probes are considered. A first-order phase transition must be accompanied by jump discontinuities in the macroscopic electronic properties. Nonetheless, to our knowledge, such discontinuities have not been observed at high temperature. Although future experiments with continuous and in situ doping tuning capability may bring important insights, the nature of this hidden "first-order transition" remains to be resolved.

Perhaps these observations signal that the incoherent strange metal is a form of matter governed by unknown emergence principles. A potential culprit is dense many-body entanglement [37]. Because the Hilbert space of a quantum many-body system grows exponentially with the system size, to compute the properties of densely entangled states in such systems is beyond the capacity of classical computers. However, because these states are delocalized in the vast Hilbert space, their excitations are generically not organized around single-particle quantum numbers and can manifest a broad spectral function [37]. This encapsulates a possible explanation for the incoherent ARPES spectra. Meanwhile, it offers a loophole for the hidden "first-order transition," as rules for transitions between densely entangled and Fermi liquid–like states are not known. Could it be that this would explain the experimental observations? We present our study as a challenge to the theory community and a potential benchmark test for quantum computing efforts.

REFERENCES ND NOTES

1. B. Keimer, S. A. Kivelson, M. R. Norman, S. Uchida, J. Zaanen, *Nature* **518**, 179–186 2015).
2. T. Timusk, B. Statt, *Rep. Prog. Phys.* **62**, 61–122 1999).
3. A. Damascelli, Z. Hussain, Z. X. Shen, *Rev. Mod. Phys.* **75**, 473–541 2003).
4. Z. X. Shen, J. R. Schrieffer, *Phys. Rev. Lett.* **78**, 1771–1774 1997).
5. Z. M. Yusof et al., *Phys. Rev. Lett.* **88**, 167006 2002).
6. A. Kaminski et al., *Phys. Rev. Lett.* **90**, 207003 2003).
7. T. Kondo et al., *Nat. Commun.* **6**, 7699 2015).
8. See supplementary materials.
9. E. Abrahams, C. M. Varma, *Proc. Natl. Acad. Sci. U.S.A.* **97**, 5714–5716 2000).
10. A. Kaminski et al., *Phys. Rev. B* **71**, 014517 2005).
11. Y. Wang et al., *Phys. Rev. Lett.* **95**, 247002 2005).
12. J. L. Tallon, J. G. Storey, J. W. Loram, *Phys. Rev. B* **83**, 092502 2011).
13. J. Corson, R. Mallozzi, J. Orenstein, J. N. Eckstein, I. Bozovic, *Nature* **398**, 221–223 1999).
14. M. Hashimoto et al., *Nat. Mater.* **14**, 37–42 2015).
15. J. L. Tallon, J. W. Loram, *Physica C* **349**, 53–68 2001).
16. J. L. Tallon, J. W. Loram, J. R. Cooper, C. Panagopoulos, C. Bernhard, *Phys. Rev. B* **68**, 180501 2003).
17. I. M. Vishik et al., *Proc. Natl. Acad. Sci. U.S.A.* **109**, 18332–18337 2012).
18. K. Fujita et al., *Science* **344**, 612–616 2014).
19. S. Badoux et al., *Nature* **531**, 210–214 2016).
20. Y. He et al., *Science* **362**, 62–65 2018).
21. F. Venturini et al., *Phys. Rev. Lett.* **89**, 107003 2002).
22. J. L. Tallon, J. W. Loram, C. Panagopoulos, *J. Low Temp. Phys.* **131**, 387–394 2003).
23. R. A. Cooper et al., *Science* **323**, 603–607 2009).
24. B. Fauqué et al., *Phys. Rev. Lett.* **96**, 197001 2006).
25. S. De Almeida-Didry et al., *Phys. Rev. B* **86**, 020504 2012).
26. L. Mangin-Thro, Y. Sidis, A. Wildes, P. Bourges, *Nat. Commun.* **6**, 7705 2015).
27. E. H. da Silva Neto et al., *Science* **343**, 393–396 2014).
28. S. Blanco-Canosa et al., *Phys. Rev. B* **90**, 054513 2014).
29. M. Hücker, N. B. et al., *Phys. Rev. B* **90**, 054514 2014).
30. Y. Sato et al., *Nat. Phys.* **13**, 1074–1078 2017).
31. J. Xia et al., *Phys. Rev. Lett.* **100**, 127002 2008).
32. L. Zhao et al., *Nat. Phys.* **13**, 250–254 2017).
33. K. M. Shen et al., *Phys. Rev. Lett.* **93**, 267002 2004).
34. T. Cuk et al., *Phys. Rev. Lett.* **93**, 117003 2004).
35. E. Kaldis et al., *Phys. Rev. Lett.* **79**, 4894–4897 1997).
36. K. Lee, S. A. Kivelson, E. A. Kim, *Phys. Rev. B* **94**, 014204 2016).
37. J. Zaanen, *SciPost Phys.* **6**, 061 2019).
38. S.-D. Chen et al. Replication data for Incoherent strange metal sharply bounded by a critical doping in Bi2212". Harvard Dataverse, Version 1 2019). https://doi.org/10.7910/DVN/VPANTG

SUPPLEMENT RY M TERI LS

science.sciencemag.org/content/366/6469/1099/suppl/DC1
Materials and Methods
Supplementary Text
Figs. S1 to S7
Table S1
References [39–45])

10 February 2019; accepted 1 November 2019
10.1126/science.aaw8850

Science

Incoherent strange metal sharply bounded by a critical doping in Bi2212

Su-Di Chen, Makoto Hashimoto, Yu He, Dongjoon Song, Ke-Jun Xu, Jun-Feng He, Thomas P. Devereaux, Hiroshi Eisaki, Dong-Hui Lu, Jan Zaanen and Zhi-Xun Shen

A sharp boundary in the cuprates

Many physicists working on cuprate superconductors believe that the so-called strange metal phase in the cuprate phase diagram is associated with a quantum critical point. Within this picture, the quantum critical point gives rise to a V-shaped region in the doping-temperature phase diagram of the cuprates: the strange metal phase. Chen *et al.* used angle-resolved photoemission spectroscopy in the cuprate family Bi2212 to challenge this view. By taking comprehensive measurements as a function of doping and temperature ––and making sure that the signal was not affected by environmental conditions––they found an incoherent strange metal phase that was sharply separated from a conventional phase by a temperature-independent vertical line in the phase diagram.
Science, this issue p. 1099

ARTICLE TOOLS	http://science.sciencemag.org/content/366/6469/1099
SUPPLEMENTARY MATERIALS	http://science.sciencemag.org/content/suppl/2019/11/25/366.6469.1099.DC1
REFERENCES	This article cites 44 articles, 6 of which you can access for free http://science.sciencemag.org/content/366/6469/1099#BIBL
PERMISSIONS	http://www.sciencemag.org/help/reprints-and-permissions

Use of this article is subject to the Terms of Service